Integrated Design and Optimization Method of an Asymmetric Hybrid Thrust Magnetic Bearing with Secondary Air-Gap

Xiaojun Ren*, **Yun Le, and Chune Wang**

Abstract—In this paper, an asymmetric thrust magnetic bearing (MB) design principle and method are introduced. Different from the general design method of magnetic bearing, the asymmetric magnetic bearing design method focuses on the effect of asymmetric factor. A permanent magnet biased asymmetric hybrid thrust magnetic bearing (AHTMB) with secondary air-gap is designed in detail. A multi-objective optimization is conducted with genetic algorithm (GA) to get smaller mass and less loss. According to optimized model parameters, magnetic field distribution, stiffness and effect of asymmetry factor on stiffness are also analyzed. For stability of the system, equivalent stiffness and equivalent damping and current characteristics are deduced. Based on the analysis results and design methods, appropriate asymmetry factor asymmetric can be chosen to satisfy the different bias force requirement. With small number of coils and current, AHTMB with secondary air-gap is beneficial for decreasing the copper loss and enhancing dynamic performance of control system.

1. NOMENCLATURE

A_{lg} Area of inner pole of lower stator.
A_{ug} Area of inner pole of upper stator.
A_{ugm} Area of middle pole of upper stator.
A_{ugo} Area of outer pole of upper stator.
B_g Bias flux density.
B_{ug} Total flux density of primary air-gap.
B_{2g} Total flux density of secondary air-gap.
b_2 Height of the secondary air gap of upper stator.
b_{s0} Width of inner pole of upper stator.
b_{sm} Width of middle pole of upper stator.
b_{s1} Width of outer pole of upper stator.
b_{pm} Height of PM.
b_{gap0} Length of inner coil window.
b_{gap1} Length of outer coil window.
d Equivalent damping.
F Magnetic force.
f_u Magnetic force of upper MB.
f_{inner} Magnetic force of inner pole of upper MB.
f_{middle} Magnetic force of middle pole of upper MB.
f_{outer} Magnetic force of outer pole of upper MB.
F_c EMF of control current.

F_{pm} MMF of the permanent magnet.
g_0 Length of air-gap.
h_1 Height of coil window.
h_2 Length of the secondary air gap of upper stator.
h_{pm} Width of PM.
h_{sum} Total height of upper stator.
$i_{\max}$ Maximal value of the coil current.
J_c Current density of coils.
k_z Displacement stiffness in z direction.
k_i Current stiffness.
k_{2g} Ratio of secondary air-gap reluctance of upper and lower MB.
k_{pm} Ratio of PM reluctance of upper and lower MB.
m Mass of upper MB.
m_c Mass of coils.
m_{pm} Mass of PM.
m_s Mass of stator.
N_c Turns number of coils.
i Control current.
R_{lg} Reluctances of the primary airgap of lower stator.
R_{g2l} Reluctances of the secondary airgap of lower stator.
R_{pm} Reluctance of PM of upper MB.
R_{pml} Reluctance of PM of lower MB.
R_s Inner radius of upper stator.
R_{ug} Reluctances of the primary airgap of upper stator.
R_{g2u} Reluctances of the secondary airgap of upper stator.
R_{ugm} Reluctances of the middle airgap of upper stator.
S_f Slot rate of coils.
V_{pm} Volume of PM.
V_c Volume of coil window.
w Total width of upper stator.
z Displacement in z direction.
σ_c Flux-leaking coefficients of the control flux.
σ_p Flux-leaking coefficients of the bias flux.
γ Asymmetry factor.
μ_0 Permeability in vacuum.
ρ_{cu} Density of coil material.
ρ_i Density of stator material.
ρ_{pm} Density of PM material.
ϕ_{cgu} Control magnetic flux of the primary airgap of the upper bearing stator.
ϕ_{cgu2} Control magnetic flux of the secondary airgap of the upper bearing stator.
ϕ_{cgl} Control magnetic flux of the primary airgap of the lower bearing stator.
ϕ_{pgl} Bias magnetic flux of the lower bearing stator.
ϕ_{pgu} Bias magnetic flux of the upper bearing stator.

2. INTRODUCTION

Magnetic bearings have numerous advantages over mechanical bearings, such as no friction, no abrasions, no lubrication, no maintenance, high speed, and high precision [1–3]. They have been widely applied in many areas, such as reaction wheels, control momentum gyros, energy storage flywheels, momentum wheels, high reliability compressors, molecular vacuum pumps, and robots [4–13].

Generally, MB structure with symmetry along the direction of the bearing force is chosen for design. Meanwhile, differential control method has often been adopted [14–20]. Because the force between the stator and rotor is always an attractive force in an active magnetic bearing (AMB), when the rotor is located in the center position without control current, the attractive forces of two magnetic bearings

are the same in the opposite directions. Therefore, the attractive forces in opposite directions offset each other, and the resultant force on the rotor is zero. When the rotor shifts under an external force, with the current control, the attractive force of one side increases while that of the opposite side decreases. The restoring force of MB makes the rotor return to center position. It can be seen that in a symmetric stator structure, the force generated by MB coil depends on current value. When the load of MB becomes large, the number of turns of the coil and the current need to be increased. Then this addition will lead to the increase of inductance of coil, which has a close relationship with the dynamic performance of a control system. Therefore, an asymmetric structure of MB is good for reducing copper consumption.

For asymmetric force implementation, there are asymmetric bias magnetic motive force (MMF), bias current, air-gap and magnetic poles. Symmetrical radial magnetic bearings generally use four or eight poles, but the three poles and six poles of an asymmetric structure have also been studied. In [21], a three-pole radial-axial hybrid magnetic bearing (HMB) was designed based on different bias and saturation flux density in radial and axial air gaps. In [22], the authors studied the control method of three-pole active magnetic bearings. They used saliency-tracking-based techniques for sensor-less control. In [23], a mathematical model of a six-pole heteropolar radial HMB was built based on an equivalent magnetic circuit. A decoupling controller was designed for the six-pole HMB. The authors found that with the same load capacity, the total power consumption of six-pole HMB was less than a traditional eight-pole active magnetic bearing. Although three poles and six poles of asymmetric structure can decrease the volume and loss, the control system was more complex. As for other asymmetric structures along the direction of the bearing force, in [24], Le et al. added a Halbatch magnetic ring to overcome the large axial load. However, it increased the axial length. As for using different air-gaps to realize nearly zero bias current control, the rotor vibration range was decreased. Therefore, we usually make the rotor located at the central position.

In the analysis of electromagnetic fields, equivalent circuit method is one of the most important methods. It has been widely used in the design and analysis of many electromagnetic devices such as MBs and motors [25–30]. To improve the performances and better meet the engineering requirements, optimization is often conducted in the design process. There are varieties of optimal methods to choose, such as GA and particle swarm optimization (PSO). GA is one of the global optimization algorithms, which has been widely used in many areas in recent years [31–33]. In [31], optimization of a robotic gripper using multi-objective GA was performed. In [32], to improve the classification performance of a polynomial neural network, a novel approach with real-coded GA was proposed. In this novel approach, the chromosome of the real-coded GA was composed of the set of partial descriptions from the first layer, the set of all input features, and a bias. In [33], the authors proposed GA and Lagrangian relaxation algorithm to solve the test selection problem of imperfect tests for fault detection and isolation.

In this paper, structure and work principle of AHTMB are firstly introduced. Secondly, design method of asymmetric magnetic bearing is deduced. The AHTMB with secondary air-gap is designed. Thirdly, after the initial design, a multi-objective optimization is conducted by genetic algorithm to get smaller mass and less loss. Finally, magnetic field distribution, current stiffness, displacement stiffness and effect of asymmetry factor on stiffness are analyzed by finite element method (FEM).

3. STRUCTURE AND WORK PRINCIPLE

### 3.1. Structure of This AHTMB

The structure of the AHTMB to be analyzed in this paper is shown in Fig. 1. MB stator is designed as a permanent magnet (PM) biased structure with secondary air-gap. The air-gap between the upper MB stator and rotor and that between the lower MB stator and rotor are equal. The area of the upper magnetic pole is larger than that of the lower magnetic pole. Hence, when the MB is in the PM bias state without applying the control current, with the same air gap magnetic density, the attractive force of the upper magnetic pole stator is larger than that of the lower magnetic pole. The resultant force of two MBs is an upward bearing force. And the bias flux provided by the PM can be used to overcome the partial load gravity. The magnitude of the load gravity is determined by the difference between the upper and lower magnetic poles.
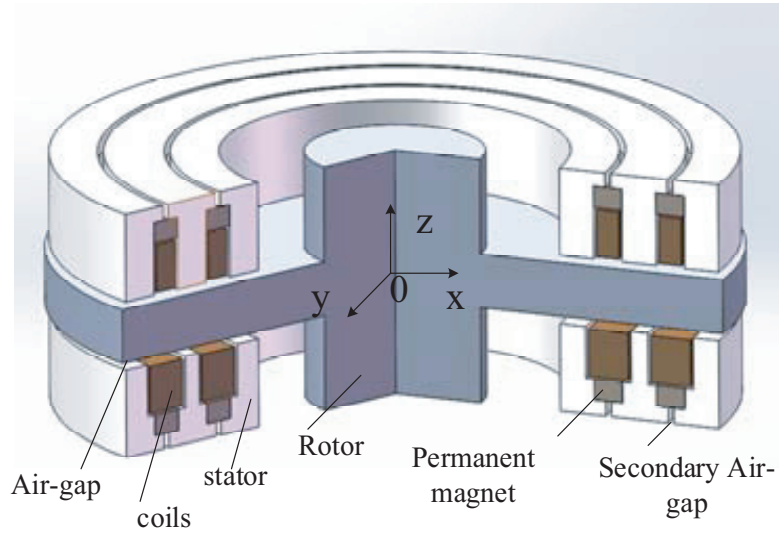
Figure 1. Structure of the AHTMB.

3.2. Work Principle of This AHTMB

When the rotor is suspended, the blue solid lines and red dashed lines in Fig. 2 denote the bias magnetic fluxes path generated by PM and control magnetic fluxes path generated by current, respectively. One part of the bias flux flies through the air-gap between stator and rotor; the other part of the bias flux passes through the secondary air-gap.
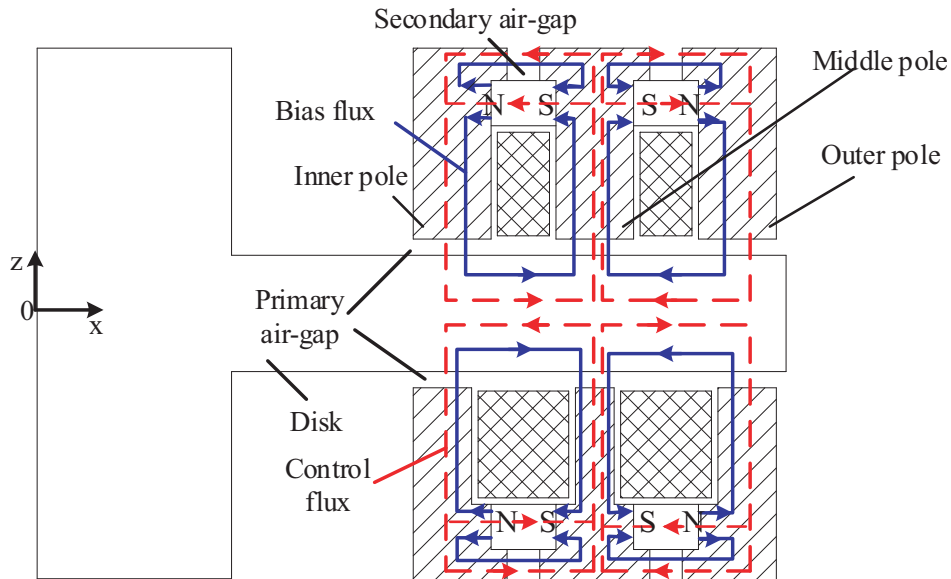
Figure 2. Bias magnetic flux and control flux path of the AHTMB.

Under load disturbance, the working principle of AHTMB is the same as the general axial MB. Rotor offset displacement is measured by sensors. Then displacement signal is sent to the controller. The controller exerts a certain control current to generate the restoring force, and finally the rotor returns to the balance position.

Differential control mode is still requested in the work of AHTMB. According to the rotor displacement detected by the sensor, the opposite currents are passed through the coils of the upper

and lower MB stators. One side bearing force becomes larger, and the other side bearing force becomes smaller. The required bearing capacity is provided by the resultant force of upper and lower MB stators.

4. ANALYSIS AND DESIGN PRINCIPLE

In order to enhance utility rate of material and decrease volume, biased magnetic density of both sides of the MB stator are designed equal to half of the maximum flux density allowed by the magnetic material. Hence, under the coil current action, the air-gap flux density of each side of the stator can be reduced to zero when the other side of magnetic flux density achieves maximum.

Assuming that the inner and outer magnetic pole areas of upper stator are A_{ug}, the middle magnetic pole area of upper stator is $2A_{ug}$; the inner and outer magnetic pole areas of lower stator are A_{lg}; the middle magnetic pole area of lower stator is $2A_{lg}$. In order to evaluate the asymmetry degree of the upper and lower MB stators, the asymmetry factor γ is defined as

$$\gamma = \frac{A_{lg}}{A_{ug}} \tag{1}$$

Obviously, the value range of γ is

$$0 < \gamma < 1 \tag{2}$$

In order to meet the conditions that the bias flux densities of the upper and lower MB stators are equal, the magnetic flux of the upper and lower bearing stators should satisfy the following relations under the permanent magnetic flux.

$$\frac{\phi_{pgl}}{\phi_{pgu}} = \frac{A_{lg}B_g}{A_{ug}B_g} = \gamma \tag{3}$$

4.1. The Analysis of the Permanent Magnetic Circuit

Due to the symmetry of magnetic circuit as shown in Fig. 2, we take the left half magnetic circuit between inner pole and middle pole of upper stator as the analysis object. In the following analysis, the reluctances of the soft magnetic materials are small enough to be ignored, and the effects of hysteresis and eddy currents are ignored as well. The leakage fluxes are represented by the flux-leaking coefficients. The equivalent magnetic circuits are shown in Fig. 3, where F_{pm} and R_{pm} are MMF and reluctance of the permanent magnet, respectively, R_{ug} is the reluctance of the inner air-gap, R_{ugm} the reluctance of the middle air-gap, R_{g2u} the reluctance of the secondary air-gap, σ_p the flux-leaking coefficients of the bias flux, which is defined as the ratios of total fluxes to efficient fluxes in the air gaps generated by PM. According to design experience, the value of σ_p is often between 1 and 2.
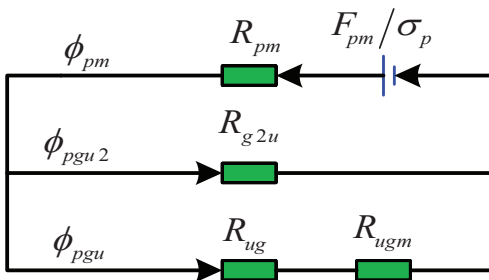
Figure 3. Equivalent magnetic circuits of bias flux.
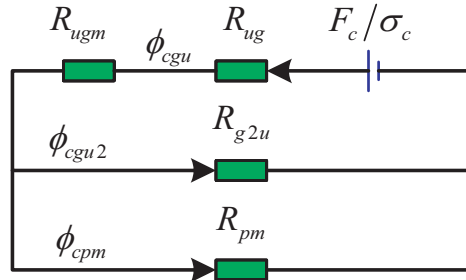
Figure 4. Equivalent magnetic circuits of control flux.

Because the middle magnetic pole area of upper stator is $2A_{ug}$, we can get $R_{ugm} = 0.5R_{ug}$. From Fig. 3, the bias fluxes of upper air-gap generated by the permanent magnet can be obtained as

$$\phi_{pgu} = \frac{F_{pm}/\sigma_p}{\left(R_{pm} + \frac{3}{2}R_{ug}\right) + \frac{3R_{pm}R_{ug}}{2R_{g2u}}} \tag{4}$$

When the lengths of upper and lower air-gaps are equal, we can get the relationship of upper and lower air-gap reluctances.

$$\frac{R_{lg}}{R_{ug}} = \frac{A_{ug}}{A_{lg}} = \frac{1}{\gamma} \tag{5}$$

where R_{dg} is the reluctance of lower air-gap.

Assume that R_{g2l} and R_{pml} are the secondary air-gap and PM reluctance of the lower MB, respectively.

$$R_{g2l} = k_{2g}R_{g2u} \tag{6}$$
$$R_{pml} = k_{pm}R_{pm} \tag{7}$$

where k_{2g} is the ratio of second air-gap reluctance of upper and lower MBs, and k_{pm} is the ratio of PM reluctance of upper and lower MBs.

Therefore, if the MMF remains unchanged, the bias fluxes of lower air-gap generated by the PM can be obtained as

$$\phi_{pgl} = \frac{F_{pm}/\sigma_p}{\left(k_{pm}R_{pm} + \frac{3}{2}\frac{R_{ug}}{\gamma}\right) + \frac{3}{2\gamma k_{2g}}\frac{k_{pm}R_{pm}R_{ug}}{R_{g2u}}} \tag{8}$$

In order to satisfy the condition that the bias magnetic flux densities of upper and lower bearing stators are equal, the bias magnetic flux in the stators of the upper and lower bearings should satisfy the following relations.

$$\frac{\phi_{pgl}}{\phi_{pgu}} = \frac{A_{lg}B_g}{A_{ug}B_g} = \gamma \tag{9}$$

Combing Eqs. (4), (8) and (9),

$$\begin{cases} k_{pm} = \dfrac{1}{\gamma} \\ \dfrac{k_{pm}}{k_{2g}\gamma} = \dfrac{1}{\gamma} \end{cases} \tag{10}$$

Therefore, the reluctance of primary air-gap, reluctance of secondary air-gap and reluctance of PM should satisfy the following relations:

$$\frac{R_{gu}}{R_{gl}} = \frac{R_{g2u}}{R_{g2l}} = \frac{R_{pm}}{R_{pml}} = \gamma \tag{11}$$

4.2. The Analysis of the Control Circuit

The equivalent magnetic circuits of control flux are shown in Fig. 4, where F_c is the MMF of the control current, which is the product of the coil number N_c and control current i; σ_c is the flux-leaking coefficient of the control flux, which is defined as the ratios of total fluxes to efficient fluxes in the air gaps generated by the control coil. According to design experience, the value of σ_c is often between 1 and 2; ϕ_{cgu} and ϕ_{cgu2} are the control fluxes of primary and secondary air-gaps, respectively; ϕ_{cpm} is the control flux passing through the PM.

The magnetic flux of upper air-gap generated by coil current can be expressed as

$$\phi_{cgu} = \frac{N_c i/\sigma_c\left(R_{pm} + R_{g2u}\right)}{\frac{3}{2}R_{gu}\left(R_{pm} + R_{g2u}\right) + R_{pm}R_{g2u}} \tag{12}$$

The corresponding air-gap flux density generated by excitation MMF can be expressed as

$$B_{cgu} = \frac{N_c i/\sigma_c\left(R_{pm} + R_{g2u}\right)}{\frac{3g_0}{2\mu_0}\left(R_{pm} + R_{g2u}\right) + R_{pm}R_{g2u}A_{gu}} \tag{13}$$

where g_0 is the length of air-gap between magnetic pole and rotor; μ_0 is the permeability in vacuum, $\mu_0 = 4\pi \times 10^{-7}$ H/m.

The area of lower stator magnetic pole, length of secondary air-gap and area of PM are changed to γ times of the corresponding values of upper end of MB. Assuming that coil turns and current are unchanged, the air-gap flux density of the lower MB under electromagnetic MMF satisfies the following relationship.

$$B_{cgl} = \frac{N_c i/\sigma_c \left(R_{pm}/\gamma + R_{g2u}/\gamma\right)}{\frac{3g_0}{2\mu_0}\left(\frac{R_{pm}}{\gamma} + \frac{R_{g2u}}{\gamma}\right) + \gamma A_{gu}\frac{R_{pm}}{\gamma} \cdot \frac{R_{g2u}}{\gamma}} = B_{cgu} \tag{14}$$

From Eq. (14), it can be seen that when the area of magnetic pole decreases, coil turns should remain the same to ensure that the flux densities of the upper and lower air-gaps are equal.

4.3. The Analysis of Force and Stiffness Characteristic

According to the above analysis, under the PM bias state, the force of the lower MB is reduced to γ times of the upper MB. Therefore, the total force of MB without applying the control current can be expressed as

$$F = (1 - \gamma)f_u \tag{15}$$

where f_u is the magnetic force of the upper MB stator. It can be expressed as

$$f_u = f_{inner} + f_{middle} + f_{outer} \tag{16}$$

where f_{inner} is the force of inner magnetic pole; f_{middle} is the force of middle magnetic pole; f_{outer} is the force of outer magnetic pole.

Since the cross area of middle magnetic pole is two times of the cross area of inner magnetic pole, and the magnetic flux densities of middle and inner magnetic poles are the same, the following can be obtained

$$f_{inner} = f_{outer} = 0.5 f_{middle} \tag{17}$$

$$f_{inner} = \frac{1}{2\mu_0 A_{gu}} \left[\frac{F_{pm}R_{g2u}/\sigma_p + N_c i\left(R_{pm} + R_{g2u}\right)/\sigma_c}{\frac{3\left(g_0 + z\right)}{2\mu_0 A_{gu}}\left(R_{pm} + R_{g2u}\right) + R_{pm}R_{g2u}} \right]^2 \tag{18}$$

When small translation z emerges in z-direction, the length of upper air-gaps g_u is changed to $(g_0 - z)$; the length of lower air-gaps g_d is changed to $(g_0 + z)$. In order to meet the needs of bearing force, differential current flies through the upper and lower coils. According to the principle of virtual work, magnetic force can be expressed as

$$F = \frac{2}{\mu_0 A_{gu}} \left[\frac{F_{pm}R_{g2u}/\sigma_p + N_c i\left(R_{pm} + R_{g2u}\right)/\sigma_c}{\frac{3\left(g_0 + z\right)}{2\mu_0 A_{gu}}\left(R_{pm} + R_{g2u}\right) + R_{pm}R_{g2u}} \right]^2$$
$$- \frac{2\gamma}{\mu_0 A_{gu}} \left[\frac{F_{pm}R_{g2u}/\sigma_p - N_c i\left(R_{pm} + R_{g2u}\right)/\sigma_c}{\frac{3\left(g_0 - z\right)}{2\mu_0 A_{gu}}\left(R_{pm} + R_{g2u}\right) + R_{pm}R_{g2u}} \right]^2 \tag{19}$$

The displacement stiffness can be obtained by the derivation of the force F for the displacement as follows:

$$k_z = \frac{\partial F}{\partial z} = -\frac{2\left(R_{pm} + R_{g2u}\right)\left[F_{pm}R_{g2u}^2/\sigma_p + N_c i\left(R_{pm} + R_{g2u}\right)/\sigma_c\right]^2}{\mu_0^2 A_{gu}^2 \left[\frac{3\left(g_0 + z\right)}{2\mu_0 A_{gu}}\left(R_{pm} + R_{g2u}\right) + R_{pm}R_{g2u}\right]^3}$$
$$- \frac{2\gamma\left(R_{pm} + R_{g2u}\right)\left[F_{pm}R_{g2u}^2/\sigma_p - N_c i\left(R_{pm} + R_{g2u}\right)/\sigma_c\right]^2}{\mu_0^2 A_{gu}^2 \left[\frac{3\left(g_0 - z\right)}{2\mu_0 A_{gu}}\left(R_{pm} + R_{g2u}\right) + R_{pm}R_{g2u}\right]^3} \tag{20}$$

The current stiffness can be obtained by the derivation of the force F for the current as follows:

$$k_i = \frac{\partial F}{\partial i} = \frac{2N_c\left(R_{pm} + R_{g2u}\right)\left[F_{pm}R_{g2u}/\sigma_p + N_ci\left(R_{pm} + R_{g2u}\right)/\sigma_c\right]}{\mu_0 A_{gu}\left[\dfrac{3\left(g_0 + z\right)}{2\mu_0 A_{gu}}\left(R_{pm} + R_{g2u}\right) + R_{pm}R_{g2u}\right]^2}$$

$$+ \frac{2\gamma N_c\left(R_{pm} + R_{g2u}\right)\left[F_{pm}R_{2gu}/\sigma_p - N_ci\left(R_{pm} + R_{g2u}\right)/\sigma_c\right]}{\mu_0 A_{ug}\left[\dfrac{3\left(g_0 - z\right)}{2\mu_0 A_{ug}}\left(R_{pm} + R_{g2u}\right) + R_{pm}R_{g2u}\right]^2} \tag{21}$$

5. OPTIMIZATION

The thrust MB designed with asymmetric structure can reduce the mass and power consumption of MBs from configuration. However, during the design process, the structure parameters of the MB also affect the bearing capacity, mass and power consumption of the MB. Therefore, in order to improve the bearing capacity and reduce the power consumption of the MB, the optimization is conducted on the bearing. Since the upper and lower MBs have symmetry degree constraint, if the parameters of upper bearing are decided, the parameters of lower MB can be calculated. Therefore, optimization is only conducted on the upper MB.

5.1. Optimization Model

5.1.1. Objective Function

Design parameters of upper MB are shown in Fig. 5. The area of inner magnetic pole can be expressed as

$$A_{ug} = \int_{R_s}^{R_s + b_{s0}} 2\pi r\, dr = \pi b_{s0}\left(2R_s + b_{s0}\right) \tag{22}$$

The area of middle magnetic pole can be expressed as

$$A_{ugm} = \int_{R_s + \frac{1}{2}w - \frac{1}{2}b_{sm}}^{R_s + \frac{1}{2}w + \frac{1}{2}b_{sm}} 2\pi r\, dr = \pi b_{sm}\left(2R_s + w\right) \tag{23}$$

The area of outer magnetic pole can be expressed as

$$A_{ugo} = \int_{R_s + w - b_{s1}}^{R_s + w} 2\pi r\, dr = \pi b_{s1}\left(2R_s + 2w - b_{s1}\right) \tag{24}$$

According to

$$A_{ug} = A_{ugo} = \frac{1}{2}A_{ugm} \tag{25}$$

Figure 5. Design variables of upper MB.

the relation among the three pole widths can be obtained.

$$b_{s1} = (R_s + w) - \sqrt{(R_s + w)^2 - 2R_s b_{s0} - b_{s0}^2} \tag{26}$$

$$b_{sm} = \frac{2(2R_s + b_{s0})b_{s0}}{2R_s + w} \tag{27}$$

The relation between two coil window widths can be obtained as

$$\begin{cases} b_{gap0} = \dfrac{w}{2} - \dfrac{b_{sm}}{2} - b_{s0} \\ b_{gap1} = \dfrac{w}{2} - \dfrac{b_{sm}}{2} - b_{s1} \end{cases} \tag{28}$$

The window space volume of MB stator coil can be expressed as

$$\begin{aligned} V_c &= \int_{R_s+b_{s0}}^{R_s+b_{s0}+b_{gap0}} 2\pi r h_1 dr + \int_{R_s+w-b_{s1}-b_{gap1}}^{R_s+w-b_{s1}} 2\pi r h_1 dr \\ &= \pi b_{gap0} h_1 (2R_s + 2b_{s0} + b_{gap0}) + \pi b_{gap1} h_1 (2R_s + 2w - 2b_{s1} - b_{gap1}) \end{aligned} \tag{29}$$

The volume of each block of permanent magnets can be expressed as

$$V_{pm} = 2\pi h_{pm} b_{pm} \left(2R_s + w + b_{s0} - b_{s1} + \frac{b_{gap0} - b_{gap1}}{2} \right) \tag{30}$$

The volume of secondary air-gap can be expressed as

$$V_{g2} = 2\pi b_2 h_2 \left(2R_s + w + b_{s0} - b_{s1} + \frac{b_{gap0} - b_{gap1}}{2} \right) \tag{31}$$

Therefore, the mass of each part of the MB can be expressed as

$$m_c = \rho_{cu} S_f V_c = \pi \rho_{cu} S_f h_1 [b_{gap0}(2R_s + 2b_{s0} + b_{gap0}) + b_{gap1}(2R_s + 2w - 2b_{s1} - b_{gap1})] \tag{32}$$

$$m_{pm} = \rho_{pm} V_{pm} = 2\pi \rho_{pm} h_{pm} b_{pm} \left(2R_s + w + b_{s0} - b_{s1} + \frac{b_{gap0} - b_{gap1}}{2} \right) \tag{33}$$

$$m_s = \rho_i [(2R_s + w)\pi w h_{sum} - V_c - V_{pm} - V_{g2}] \tag{34}$$

where m_c, m_{pm} and m_s are the mass of the coils, PM and stator, respectively; S_f is coil slot full rate.

The total mass of the upper MB is

$$m = m_c + m_{pm} + m_s \tag{35}$$

The copper consumption of the asymmetric axial MB can be obtained according to the Ohm's law by the coil current and the resistance. Coil current can be obtained by the product of cross sectional area and coil current density. The resistance of coil can be represented by the relevant parameters of the coil window.

$$i_{\max} = J_c A_c = J_c b_{gap0} h_1 S_f / N_c \tag{36}$$

The coil resistance can be expressed as the structural parameters of the MB

$$R_{cu} = \frac{2\pi \rho N_c (2R_s + 2b_{s0} + b_{gap0})}{b_{gap0} h_1 S_f / N_c} \tag{37}$$

Therefore, the copper consumption of the MB in the maximum bearing capacity is

$$P = 2\pi \rho J_c^2 b_{gap} h_1 S_f (2R_s + 2b_{s0} + b_{gap0}) \tag{38}$$

Therefore, the objective function of the asymmetric axial MB in the optimization process can be determined as

$$\begin{cases} \min \ m = m_c + m_{pm} + m_s \\ \min \ P = 2\pi \rho J_c^2 b_{gap0} h_1 S_f (2R_s + 2b_{s0} + b_{gap0}) \end{cases} \tag{39}$$

Table 1. Structure parameters.

Parameters	value
Length of inner coil window	b_{gap0}
Length of outer coil window	b_{gap1}
Length of PM	h_{pm}
Height of coil window	h_1
Length of secondary air-gap	h_2
Height of stator	h_{sum}
Height of PM	b_{pm}
Height of secondary air-gap	b_2
Length of stator	w
Width of inner magnetic pole	b_{s0}
Width of outer magnetic pole	b_{s1}
Width of middle magnetic pole	b_{sm}
Radius of inner stator	R_S
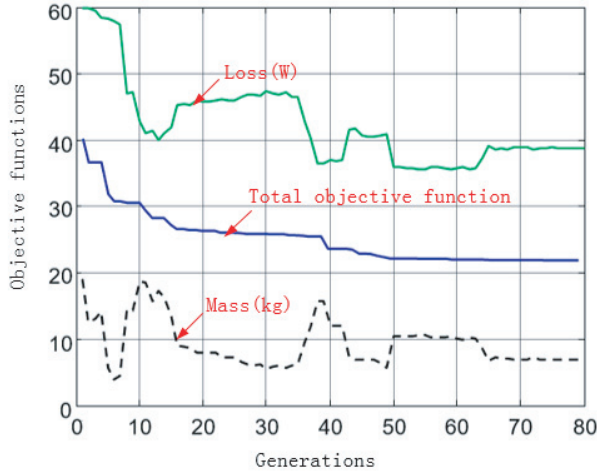
Figure 6. Optimization trend of the objective function with the genetic evolution.
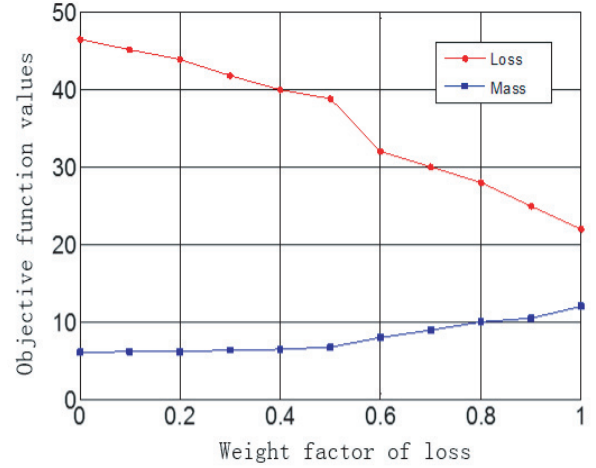
Figure 7. Mass and loss versus loss weight factor.

5.1.2. Selection of Design Variables

The design structure parameters are shown in Fig. 7 and Table 1, where b_{gap0}, b_{gap1}, h_{pm}, h_1, h_2, h_{sum}, b_{pm}, b_2, w, b_{s0}, b_{s1}, b_{sm} and R_S are design variables.

According to Eqs. (16), (17) and (18), f_u can be expressed as

$$f_u = \frac{2}{\mu_0 A_{gu}} \left[\frac{F_{pm}R_{2gu}/\sigma_p + N_c i \left(R_{pm} + R_{2gu}\right)/\sigma_c}{\dfrac{3\left(g+z\right)}{2\mu_0 A_{gu}} \left(R_{pm} + R_{2gu}\right) + R_{pm}R_{2gu}} \right]^2 \tag{40}$$

From Eq. (40), it can be seen that the bearing force f_u can be regarded as a nonlinear function of the second air-gap reluctance R_{2gu}. In order to get the maximum value of f_u, the derivation of the force f_u for R_{2gu} can be obtained as follows:

$$\frac{\partial f_u}{\partial R_{g2u}} = 0 \tag{41}$$

After a series of simplified calculation, the optimal value of the secondary air-gap reluctance can be expressed as

$$R_{g2u} = \frac{3R_{pm}R_{ug}}{2R_{pm} - 3R_{ug}} \tag{42}$$

Seen from Eq. (42), the optimal value of the secondary air-gap reluctance is only related to the reluctance of the PM R_{pm} and air gap reluctance R_{gu}. It has nothing to do with MMF of PM and coils. Therefore, the parameters of secondary air-gap can be determined by the size of permanent magnet and the air gap. In this way, it can reduce the number of parameters involved in the design of MBs and simplify the optimization process.

The relationship between the secondary air-gap reluctance and the related structural parameters can be expressed as

$$R_{g2u} = \frac{h_2}{2\pi\mu_0 b_2 \left(R_s + b_{so} + 0.5b_{gap0}\right)} \tag{43}$$

Combining Eqs. (39) and (40), we can calculate

$$h_2 = \frac{3R_{pm}R_{ug}}{2R_{pm} - 3R_{ug}} \cdot 2\pi\mu_0 b_2 \left(R_s + b_{so} + 0.5b_{gap0}\right) \tag{44}$$

where

$$R_{pm} = \frac{h_{pm}}{2\pi\mu_0\mu_r b_{pm} \left(R_s + b_{so} + 0.5b_{gap0}\right)} \tag{45}$$

$$R_{gu} = \frac{g_0}{2\pi\mu_0 b_{so} \left(R_s + 0.5b_{so}\right)} \tag{46}$$

For width and height of the MB stator, the structural parameters satisfy the relationship

$$w = b_{so} + b_{gap_0} + b_{sm} + b_{gap_1} + b_{s1} \tag{47}$$

$$h_{sum} = b_2 + b_{pm} + h_1 \tag{48}$$

Combining Eqs. (23), (24), (25) and (44), it can be seen that b_{gap0}, b_{sm}, b_{gap1} and b_{s1} can be expressed by other parameters. From Eq. (48), it can be seen that h_1 can be expressed by other parameters. In order to ensure that the coil temperature is in a certain range, the current density of the coil cannot be too large. Hence, the design of the coil current density should be one of the optimization variables.

Based on the analysis above, the optimal design variables in the optimization are as follows:

$$x = [w, b_{so}, b_2, b_{pm}, h_{pm}, h_{sum}, J_c] \tag{49}$$

The design region is listed in Table 2. The bearing is designed for a magnetically suspended inertially stabilized platform. The structure and total volume range of the platform limite the design space of magnetic bearing. The axial length of the magnetic bearing is limited by the rotor mode. The upper bounds of w, b_{s0}, b_2, b_{pm}, h_{pm} and h_{sum} are obtained. Taking into account the feasibility of the processing and easy assembly, the lower limits of w, b_{s0}, b_2, b_{pm}, h_{pm} and h_{sum} are gained by design experience. For example, in order to provide sufficient bias magnetic density and to ensure that the

Table 2. Region of design variables.

design variable	Initial design	Lower limit	Upper bound
w	55 mm	45 mm	65 mm
b_{s0}	6 mm	5 mm	10 mm
b_2	3 mm	1 mm	4 mm
b_{pm}	4 mm	3 mm	7 mm
h_{pm}	20 mm	15 mm	25 mm
h_{sum}	20 mm	15 mm	30 mm
J_C	4 A/mm^2	2 A/mm^2	5 A/mm^2

processing of PM is easy, the lower limit of PM magnetization length h_{pm} is set at 15 mm. The boundary value of J_c is determined by the requirement of control current and the safe current density limitations of coils.

5.2. Constraints

The constraint condition of the asymmetric axial MB in the optimization process mainly includes the load capacity of the MB and the magnetic flux density of each part of the core. In order to suspend the rotor, MB force has to not only overcome gravity load but also overcome the negative stiffness force. Therefore, for the design of MBs, the maximum load capacity of the MB should be limited. When the rotor is started to levitate, the air-gap flux density of upper stator will achieve the maximum value. In an ideal situation, air-gap flux density of lower stator is reduced to zero. Therefore, for the air gap of lower magnetic pole, the resultant magnetic flux density of PM bias and control magnetic flux density can be expressed as follows:

$$B_{gd} = \frac{\gamma \left(F_{pm}/\sigma_p\right) R_{2gu}}{R_{pm}R_{2gu}A_{gu} + 2\left(g - z\right)\left(R_{pm} + R_{2gu}\right)/\mu_0} - \frac{\gamma N_c i/\sigma_c \left(R_{pm} + R_{2gu}\right)}{2\left(g - z\right)\left(R_{pm} + R_{2gu}\right)/\mu_0 + R_{pm}R_{2gu}A_{gu}} = 0 \quad (50)$$

From Eq. (50), the relationship of permanent magnet MMF and electromagnetic MMF can be obtained

$$F_{pm} = \frac{N_c i \left(R_{pm} + R_{2gu}\right) \sigma_p}{\sigma_c R_{2gu}} \quad (51)$$

According to the design requirements of the load capacity of the platform, the maximum force of the MB is

$$F_{\max} = \frac{4}{\mu_0 A_{ug}} \left[\frac{\left(2F_{pm}/\sigma_p\right) R_{g2u}}{R_{pm}R_{g2u} + R_{ug}\left(R_{pm} + R_{g2u}\right)}\right]^2 \geq 1200\,\text{N} \quad (52)$$

Taking the magnetic saturation of the material into account, the saturation value of the ferromagnetic material B_{sat} is about 1.2 T. In order to ensure that the core material works in the linear region of the BH curve, the work maximum magnetic density of the material should be less than the saturated magnetic density of the material. Therefore, magnetic flux density constraint conditions are expressed as follows:

$$B_{ug} = \frac{\left(2F_{pm}/\sigma_p\right) R_{g2u}}{R_{pm}R_{g2u}R_{ug} + 2(g_0 + z)(R_{pm} + R_{g2u})/\mu_0} \leq 1.2\,\text{T} \quad (53)$$

$$B_{2g} = \frac{F_{pm}}{A_{g2u}\sigma_p \left(R_{pm} + R_{g2u}\right)} \leq 1.2\,\text{T} \quad (54)$$

5.3. Optimization Algorithm

Optimization of asymmetric PM biased axial MB is a complex multi-variable, nonlinear, multi-objective optimization problem. For traditional optimization methods, optimization effect is related to the position of initial point, and generally optimization result converges to a local optimal value [33]. Here, we choose the global optimization GA. GA has two ways to process constraints. One is to add an amending operator, and the other is to use a penalty function. In this paper, we take the latter.

According to Eq. (39), the optimization objective function of the asymmetric axial MB is given, which is the mass and power consumption. Combining with the weight coefficient w_1 and w_2, the evaluation function can be constructed as follows:

$$f = w_1 m + w_2 p, \quad (w_1 + w_2 = 1) \quad (55)$$

Taking f as a new optimization goal, combing with Table 2 and Eqs. (52), (53), (54), a viable optimization space of variables and constraint items can be obtained. Here, the values of w_1 and w_2 are equal to 0.5. The parameters of genetic algorithm are very important to the calculation results of genetic algorithm. The computational complexity of genetic algorithm is directly influenced by the population size and genetic algebra.

5.4. Optimization Results Analysis

The variation trend of the total objective function, mass and loss of the MB in the optimization process is shown in Fig. 6. It can be seen from Fig. 6 that when the number of generations is larger than 64, the values of total objective function, mass and loss of the MB become relatively stable. When genetic algorithm finds the optimal value in the global scope, the mass of MB is 8 kg, which is 42% of initial value; the loss of MB is 39 W, which is 65% of initial value. The mass and loss of MB are not respective minimum values, because mass and loss are two mutually contradictory characteristics, so they cannot achieve the minimum values at the same time. Optimal values of mass and loss with different weight factors are shown in Fig. 7.

It can be seen from Fig. 7 that with the increase of loss weight factor, the optimal value of loss is decreased and the optimal value of mass increased. But when the loss weight factor is less than 0.5, the increasing trend of the mass is not very obvious. In order to satisfy certain conditions, such as bearing capacity, magnetic field density requirements and so on, pole area cannot be infinitely reduced, and windings window cannot be decreased infinitely, so after mass reaches a certain value, it will not be decreased infinitely. Considering the variation trend of loss and mass, weight factors of both the objects are 0.5.

According to the optimization results, the design parameters of upper MB are finally determined as shown in Table 3.

Table 3. Optimization results of design parameters.

| Parameters	value
Axial air gap length, g_0, mm	0.4
Outer radius of the rotor, r_0, mm	15
Inner radius of the upper stator, R_s, mm	30
width of the upper stator, w, mm	60
Height of upper stator, h_{sum}, mm	25
Width of inner pole of upper stator, b_{s0}, mm	8
Width of middle pole of upper stator, b_{sm}, mm	9
Area of magnetic pole, $A_{\lg}$, mm^2	1700
Length of PM magnetization, h_{pm}, mm	16
Height of PM, b_{pm}, mm	5
Length of secondary air-gap, h_2, mm	4
Height of secondary air-gap, b_2, mm	2
Width of inner coil window, b_{gap0}, mm	17
Width of outer coil window, b_{gap1}, mm	22
Height of coil window, h_1, mm	18
Current density, J_c, A/ mm^2	3
Relative permeability of PM, μ_r	1.05
Coercive force of PM2, kA/m, H_C	796
Maximum number of ampere turns, $N_c i_c$	200

5.5. Design Parameters of Lower Bearing

According to the bearing size optimization results and previous analysis of upper and lower bearings on symmetry constraints, we can calculate the next dimension parameters of the bearing shown in Fig. 8.

5.5.1. Calculation of Pole Width

According to Eq. (5), we can get

$$b_{sol} = \gamma b_{s0}, \quad b_{sml} = \gamma b_{sm}, \quad b_{s1l} = \gamma b_{s1} \tag{56}$$
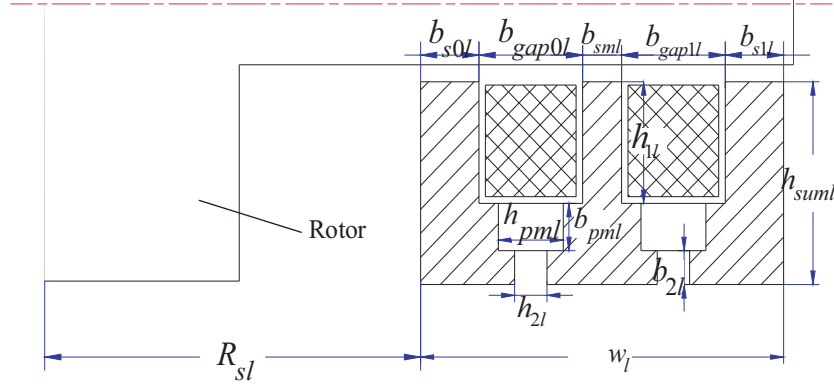
Figure 8. Design parameters of lower MB.

5.5.2. Calculation of Inner Radius of the Lower Stator and Length of the Lower Stator

According to the geometric and symmetrical relationship, inner radius of the lower stator and length of the lower stator can be calculated as follows

$$\begin{cases} R_{sl} = R_s + (1 - \gamma)b_{s0} \\ w_l = w - (1 - \gamma)b_{s0} - (1 - \gamma)b_{s1} \end{cases} \tag{57}$$

5.5.3. Calculation of Permanent Magnets Parameters

According to Eq. (11), we can get

$$\frac{R_{pm}}{R_{pml}} = \frac{h_{pm}A_{pml}}{h_{pml}A_{pm}} = \gamma \tag{58}$$

Because previous analysis assumes that MMFs of permanent magnets of the upper and lower bearings are the same, and the same material is used, length of magnetization of the upper and lower bearing permanents should be equal.

$$h_{pml} = h_{pm} \tag{59}$$

Substituting Eq. (59) into Eq. (58) for the same part, we can get

$$\frac{A_{pml}}{A_{pm}} = \frac{b_{pml}}{b_{pm}} = \gamma \tag{60}$$

Therefore, the height of the permanent magnet can be calculated as

$$b_{pml} = \gamma b_{pm} \tag{61}$$

5.5.4. Calculation of Secondary Air-Gap Parameters

According to Eq. (11), we can get

$$\frac{R_{2g}}{R_{2gl}} = \frac{h_2 A_{2gl}}{h_{2l} A_{2gu}} = \gamma \tag{62}$$

The geometric centers of the secondary air gaps of upper and lower bearings are kept the same. Heights of the secondary air-gaps are the same which means

$$b_{2l} = b_2 \tag{63}$$

Hence, we can get

$$A_{2gl} = A_{2gu} \tag{64}$$

Substituting Eq. (64) into Eq. (63) for the same part, we can get

$$h_{2l} = \frac{1}{\gamma}h_2 \tag{65}$$

5.5.5. Calculation of Coil Window Size and the Total Height of the Stator

According to Eq. (28), we can calculate the window size

$$\begin{cases} b_{gap0l} = \dfrac{w_l}{2} - \dfrac{b_{sml}}{2} - b_{s0l} \\ b_{gap1l} = \dfrac{w_l}{2} - \dfrac{b_{sml}}{2} - b_{s1l} \end{cases} \tag{66}$$

Height of the coil window of lower MB is consistent with height of the coil window of upper MB. That means

$$h_{1l} = h_1 \tag{67}$$

Therefore, the overall height of the lower bearing stator can be expressed as

$$h_{suml} = b_{2l} + b_{pml} + h_{1l} \tag{68}$$

In summary, the final design parameters of the lower MB are shown in Table 4.

Table 4. Design parameters of lower MB.

Parameters	value
Asymmetry factor, γ	50%
Axial air gap length, g_0, mm	0.4
Outer radius of the rotor, r_0, mm	15
Inner radius of the upper stator, R_{sl}, mm	34
width of the upper stator, w_l, mm	54.5
Height of upper stator, h_{suml}, mm	22.5
Width of inner pole of upper stator, b_{s0l}, mm	4
Width of middle pole of upper stator, b_{sml}, mm	9
Area of magnetic pole, A_{gl}, mm^2	850
Length of PM magnetization, h_{pm}, mm	16
Height of PM, b_{pml}, mm	2.5
Length of secondary air-gap, h_{2l}, mm	8
Height of secondary air-gap, b_{2l}, mm	2
Width of inner coil window, b_{gap0l}, mm	21
Width of outer coil window, b_{gap1l}, mm	23
Height of coil window, h_{1l}, mm	18
Current density, J_c, A/mm^2	3
Relative permeability of PM, μ_r	1.05
Coercive force of PM2, kA/m, H_C	796
Maximum number of ampere turns, $N_c i_c$	200

6. SIMULATION

Based on the parameters listed in Tables 3 and 4, the simulation mode is constructed. The FEM method is used to analyze the distribution of the flux density, the relationship between magnetic force and displacement, the relationship between magnetic force and control current, and the relationship between the stiffness and asymmetry factor.

6.1. Magnetic Field Distribution

Fig. 9 shows the bias magnetic flux density of this AHTMB when the rotor is located at the equilibrium position. From Fig. 9, it can be seen that the bias magnetic flux density of upper air-gaps is about 0.7 T.
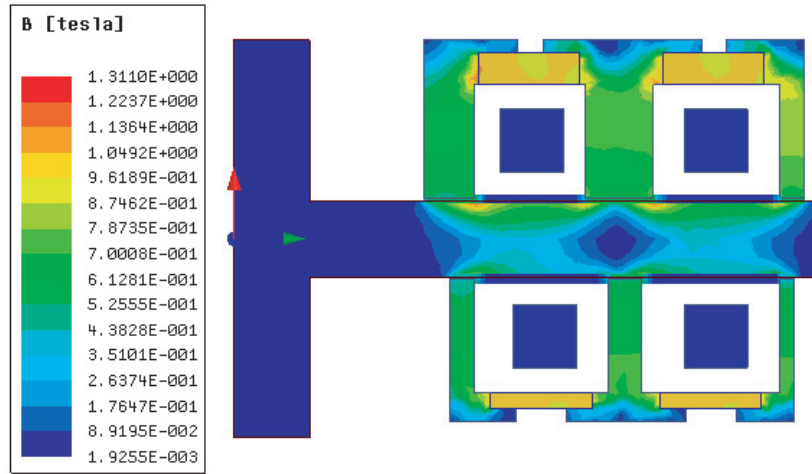
Figure 9. Distribution of bias flux density at the equilibrium position.

There is a little difference in the bias density between the upper and lower air gaps. That is because some approximations have been made in the previous calculation. Although the difference between the bias magnetic flux densities of upper and lower air gaps is small, due to different pole areas, the resultant force is about 400 N.

6.2. Current Stiffness and Displacement Stiffness

The force-displacement relations of the MB are shown in Fig. 10(a). It can be seen that when rotor is located at the central equilibrium position, the magnetic force is nearly proportional to the displacement. The force-displacement stiffness without current can be calculated as about $-2400 \, \text{N/mm}$ Fig. 10(a).

The force-current relations of the MB are shown in Fig. 10(b). It can be seen that the magnetic force is nearly proportional to the current. The force-current stiffness without displacement can be calculated as about $1250 \, \text{N/A}$ from Fig. 10(b).
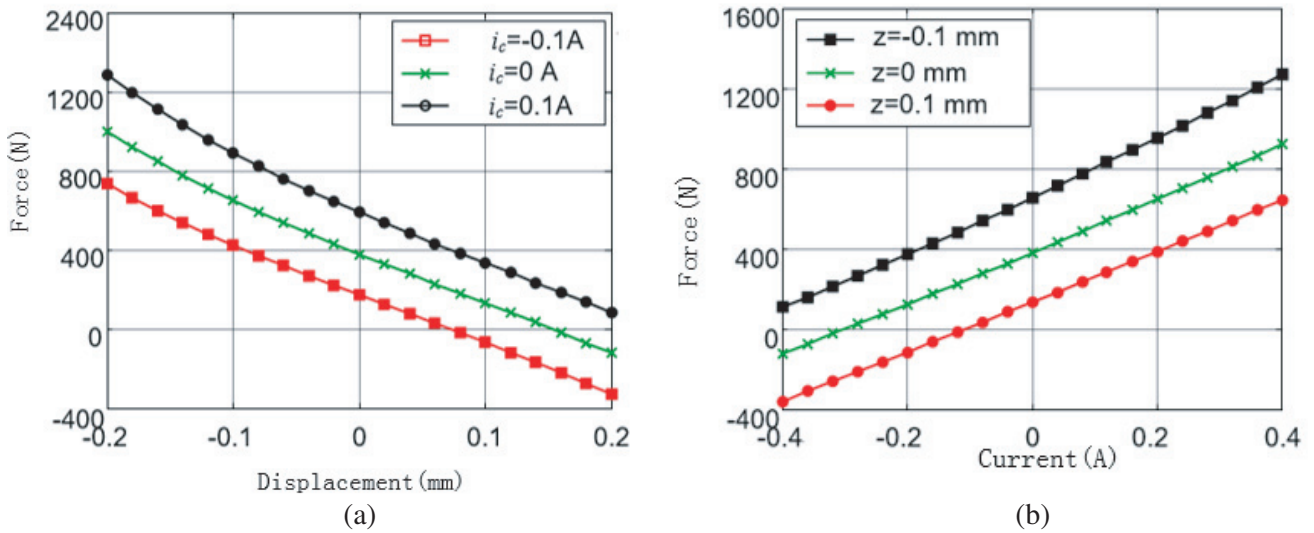

Figure 10. Stiffness curve. (a) Force-displacement characteristic curve. (b) Force-current characteristic curve.

It can be seen in Fig. 10 that due to the asymmetrical structural, when the value of current and displacement is 0, the bearing force is 400 N. Therefore, when the rotor is located at the central equilibrium position, with very small control current, biased magnetic flux can provide a bearing force to overcome the partial load gravity.

6.3. Effect of Asymmetry Factor γ on Stiffness

With different displacements and different currents, Fig. 11(a) shows the effect of asymmetry factor γ on current stiffness. Fig. 11(b) shows the effect of asymmetry factor γ on displacement stiffness under different currents and displacements. $\gamma = 1$ denotes that lower MB has same size as upper MB. $\gamma = 0$ denotes that AHTMB only has the upper MB and does not have lower MB.
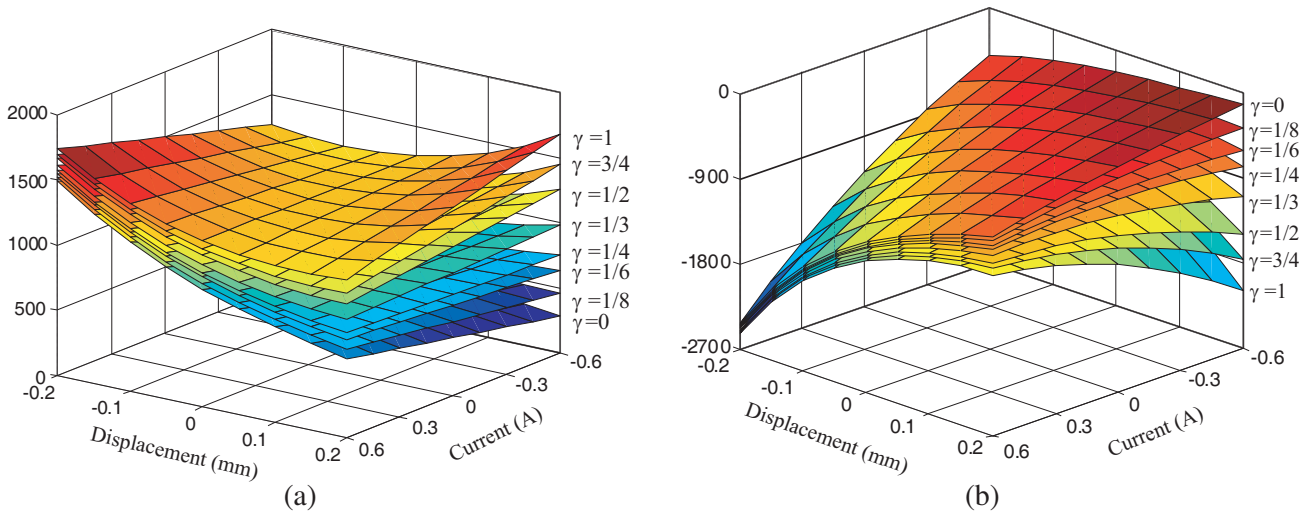
Figure 11. Effect of asymmetry factor γ on stiffness. (a) Effect on current stiffness. (b) Effect on displacement stiffness.

It can be seen from Fig. 11(a) that the current stiffness of the MBs is no longer symmetric about the magnetic center. When the rotor moves to the upper magnetic pole area, the MB's current stiffness is increased significantly. As shown in Fig. 11(b), in this asymmetric structure, the displacement of the MBs is no longer symmetric about the magnetic center, too. The maximum displacement is at somewhere of the displacement of more than zero.

7. CONCLUSION

In this paper, asymmetric MB design methods are introduced. AnAHTMB with secondary air-gap is designed. After a multi-objective optimization with GA, the mass is decreased to 42% and loss decreased to 65% of the initial value. In order to avoid the saturation of a magnetic pole in advance, the design keeps magnetic flux density of all poles in one direction. The stability of the system can be realized by adjusting the stiffness and damping of the control. Due to the asymmetric structure, the current and displacement stiffness of the MBs is no longer symmetric about the center. The current stiffness is increased significantly when rotor is close to the upper MB. Based on the analysis results and design methods, appropriate asymmetric factor can be chosen to satisfy the different bias force requirement. This design method focusing on the effects of asymmetric factors has important value in the design of asymmetric MBs.

ACKNOWLEDGMENT

REFERENCES

1. Ren, X. J., Y. Le, and B. C. Han, "Asymmetric electromagnetic analysis and design of a permagnet biased axial magnetic bearings," *Progress In Electromagnetics Research Symposium*, 574–586, Shanghai, China, August 8–11, 2016.

2. Eaton, D., J. Rama, and S. Singhal, "Magnetic bearing applications & economics," *Proc. PCIC*, 1–9, September 2010.

3. Ren, X. J., Y. Le, and B. C. Han, "System electromagnetic loss analysis and temperature field estimate of a magnetically suspended motor," *Progress In Electromagnetics Research M*, Vol. 55, 51–61, 2017.

4. Eaton, D., J. Rama, and S. Singhal, "Magnetic bearing applications & economics," *Proc. PCIC*, 1–9, September 2010.

5. Betschon, F., *Design Principles of Integrated Magnetic Bearings*, Swiss Federal Institute of Technology, Zurich, 2000.

6. Han, B. C., S. Q. Zheng, Y. Le, et al., "Modeling and analysis of coupling performance between passive magnetic bearing and hybrid magnetic radial bearing for magnetically suspended flywheel," *IEEE Trans. Magn.*, Vol. 49, No. 10, 5356–5370, 2013.

7. Le, Y., J. Fang, and J. Sun, "An integrated passive magnetic damping system for high-speed compressor with flexible rotor," *Proc. ImechE, Part C: J. Mechanical Engineering Science*, Vol. 229, No. 6, 1150–1161, 2015.

8. Fang, J., C. Wang, and J. Tang, "Modeling and analysis of a novel conical magnetic bearing for vernier-gimballing magnetically suspended flywheel," *Proc. ImechE, Part C: J Mechanical Engineering Science*, Vol. 228, No. 13, 2416–2425, 2014.

9. Fang, J. C., S. Q. Zheng, B. C. Han, et al., "AMB vibration control for structural resonance of double-gimbal control moment gyro with high-speed magnetically suspended rotor," *IEEE Transactions on Mechatronics*, Vol. 18, No. 1, 32–43, 2013.

10. Zheng, S. Q., B. C. Han, L. Guo, et al., "Composite hierarchical antidisturbance control for magnetic bearing system subject to multiple external disturbances," *IEEE Transactions on Industrial Electronics*, Vol. 61, No. 12, 7004–7012, 2014.

11. Fang, J. C., Y. Le, J. J. Sun, and K. Wang, "Analysis and design of passive magnetic bearing and damping system for high-speed compressor," *IEEE Trans. Magn.*, Vol. 48, No. 9, 2528–2537, 2012.

12. Noh, M. D., S. Cho, J. Kyung, S. Ro, and J. Park, "Design and implementation of a fault-tolerant magnetic bearing system for turbo-molecular vacuum pump," *IEEE/ASME Trans. Mech.*, Vol. 10, No. 6, 626–631, 2005.

13. Selmy, M., M. Fanni, and A. M. Mohamed, "Design and control of a novel contactless active robotic joint using AMB," *2015 IEEE International Conference on Autonomous Robot Systems and Competitions (ICARSC)*, 144–149, December 2015.

14. Ren, X. J., Y. Le, J. J. Sun, et al., "Magnetic flux leakage modeling and optimization of a combined radial-axial hybrid magnetic bearing for DC motor," *IET Electric Power Applications*, Vol. 17, No. 2, 212–221, 2017.

15. Liu, X. X., J. Y. Dong, Y. Du, et al., "Design and static performance analysis of a novel axial hybrid magnetic bearing," *IEEE Trans. Magn.*, Vol. 50, No. 11, 8300404, 2014.

16. Zhang, W. and H. Zhu, "Improved model and experiment for AC-DC three-degree-of-freedom hybrid magnetic bearing," *IEEE Trans. Magn.*, Vol. 49, No. 11, 5554–5565, 2013.

17. Bachovchin, K. D., J. F. Hoburg, and R. F. Post, "Magnetic fields and forces in permanent magnet levitated bearings," *IEEE Trans. Magn.*, Vol. 48, No. 7, 2112–2120, 2012.

18. Fang, J. C., X. Wang, T. Wen, et al., "Homopolar 2-pole radial permanent-magnet biased magnetic bearing with low rotating loss," *IEEE Trans. Magn.*, Vol. 48, No. 8, 2293–2303, 2012.

19. Eryong, H. and L. Kun, "Investigation of axial carrying capacity of radial hybrid magnetic bearing," *IEEE Trans. Magn.*, Vol. 48, No. 1, 38–46, 2012.

20. Eryong, H. and L. Kun, "A novel structure for low-loss radial hybrid magnetic bearing," *IEEE Trans. Magn.*, Vol. 47, No. 12, 4725–4733, 2011.

21. Zhu, H. and J. Ju, "Design and optimisation of three-pole radial-axial HMB with independent radial and axial carrying capacity," *2015 IEEE Magnetics Conference (INTERMAG)*, Beijing, May 11–15, 2015.

22. Garcia, P., J. M. Guerrero, F. Briz, et al., "Sensorless control of three-pole active magnetic bearings using saliency-trackingbased methods," *IEEE Trans. Ind. Appl.*, Vol. 46, No. 4, 1476–1484, 2010.

23. Ji, L., L. X. Xu, and C. W. Jin, "Research on a low power consumption six-pole heteropolar hybrid magnetic bearing," *IEEE Trans. Magn.*, Vol. 49, No. 8, 4918–4926, 2013.

24. Le, Y., J. C. Fang, and J. J. Sun, "Design of a halbach array permanent magnet damping system for high speed compressor with large thrust load," *IEEE Trans. Magn.*, Vol. 51, No. 1, 8300109, 2015.

25. Tomczuk, B., J. Zimon, and D. Wajnert, "Eddy current influence on the parameters of the active magnetic bearing," *Proceedings of the 12th International Symposium on Magnetic Bearings*, 267–272, Wuhan, China, August 22–25, 2010.

26. Zimon, J., B. Tomczuk, and D. Wajnert, "Field-circuit modeling of AMB system for various speeds of the rotor," *Journal of Vibroengineering*, Vol. 14, 165–170, March 2012.

27. Tomczuk, B., D. Wajnert, and J. Zimon, "Influence of bias current value on properties of active magnetic bearing," *Solid State Phenomena*, Vol. 198, 513–518, 2013.

28. Tomczuk, B., J. Zimon, and D. Wajnert, "Field-circuit modeling of the 12-pole magnetic bearing characteristics," *Proceedings of Compumag. 2013*, Budapest, Hungary, June 30–July 4, 2013.

29. Wajnert, D. and B. Tomczuk, "Simulation for the determination of the hybrid magnetic bearing's electromagnetic parameters," *Electrical Review*, 157–160, Poland, (Przegląd Elektrotechniczny), ISSN 0033-2097, R. 93 NR 2/2017.

30. Gieras, J. F., Z. J. Piech, and B. Z. Tomczuk, *Linear Synchronous Motors*, Taylor & Francis, USA, 2012.

31. Datta, R., S. Pradhan, and B. Bhattacharya, "Analysis and design optimization of a robotic gripper using multiobjective genetic algorithm," *IEEE Transactions on Systems, Man, and Cybernetics: Systems*, Vol. 46, No. 1, 16–26, 2016.

32. Lin, C. T., M. Prasad, and A. Saxena, "An improved polynomial neural network classifier using real-coded genetic algorithm," *IEEE Transactions on Systems, Man, and Cybernetics: Systems*, Vol. 45, No. 11, 1389–1401, 2015.

33. Zhang, S. G., K. R. Pattipati, Z. Hu, et al., "Optimal selection of imperfect tests for fault detection and isolation," *IEEE Transactions on Systems, Man, and Cybernetics: Systems*, Vol. 43, No. 6, 1370–1384, 2013.